Supporting Information

Transition-Metal Embedded gt-C_3N_3 Monolayers: High-Temperature Ferromagnetism and High Anisotropy

Indrani Choudhuri,[†] Priyanka Garg,[†] Biswarup Pathak,[†,#,*]

[†]Discipline of Chemistry and [#]Discipline of Metallurgy Engineering and Material Science, Indian Institute of Technology (IIT) Indore, Indore 453552, India

Email: biswarup@iiti.ac.in

Contents:

Figure S1: (a) Optimized structure of gt-C_3N_3 (top and side views) and (b) charge density of gt-C_3N_3 (Isosurface value is 0.18 e.Å^{-3}).

Figure S2: Optimized structures (top and side views) of TM@gt-C_3N_3 (TM = Sc to Cu) structures.

Table S1: Bond lengths and net effective charges calculated from Bader Charge analysis of gt-C_3N_3 and TM@gt-C_3N_3 (See Figure 1 in the manuscript for atom numbering)

Text S1. Formation Energy (E_f), Binding Energy (E_B) and Cohesive Energy (E_{coh}) calculations.

Figure S3: Total electron density (Isosurface value: 0.18 e.Å^{-3}) and electrostatic potentials (ESP) plots (Isosurface value: 0.03 e.Å^{-3}) of TM@gt-C_3N_3 (Sc to Cu). The blue and red colours denote less and more electron dense area in the electrostatic potential surface.

Table 2: Binding energy (E_B/TM), formation energy (E_F), cohesive energy of TM bulk (E_{Coh}/atom) and phonon frequency of TM@gt-C_3N_3 systems. (TM = Sc to Cu)

Figure S4: Phonon band structures of TM@gt-C_3N_3 (TM = Sc to Cu)

Figure S5: Total energy fluctuation during AIMD simulations of Cr@gt-C_3N_3, Mn@gt-C_3N_3 and Fe@gt-C_3N_3 systems at 400 and 500 K. The structures represent the snapshot at 10 ps for each simulation.

Figure S6: Strain energy of (a) Cr@gt-C_3N_3 (b) Mn@gt-C_3N_3 and (c) Fe@gt-C_3N_3 under in-plane uniaxial and equi-biaxial strains.

Table S3: Calculated Young's Modulus and Poisson's ratio of TM@gt-C_3N_3 by applying uniaxial and equi-biaxial strain.

Figure S7. Energy diagram of d-orbital splitting of different TM@C_3N_3 systems.

Figure S8: (a) TDOS and pDOS plot of (a) Cr@gt-C_3N_3, (b) Mn@gt-C_3N_3 and (c) Fe@gt-C_3N_3 (Fermi level is shifted to zero and indicated by black dashed line)

Table S4: Exchange energy (E_{ex}) and Curie temperature value of TM@gt-C_3N_3 system.

Figure S9. Band structures of Mn@gt-C_3N_3 by applying 1%, 5% and 10% (a) uniaxial and (b) biaxial tensile strain. The Fermi level is set to zero and indicated by blue dashed line.

Figure S10. Band structures of Fe@gt-C_3N_3 by applying 1%, 5% and 10% (a) uniaxial and (b) biaxial tensile strain. The Fermi level is set to zero and indicated by blue dashed line

Text S2. Calculation of Magnetic Anisotropy Energy (MAE)

Text S3. Mean Field Theory (MFT) and Monte Carlo Simulation.

References

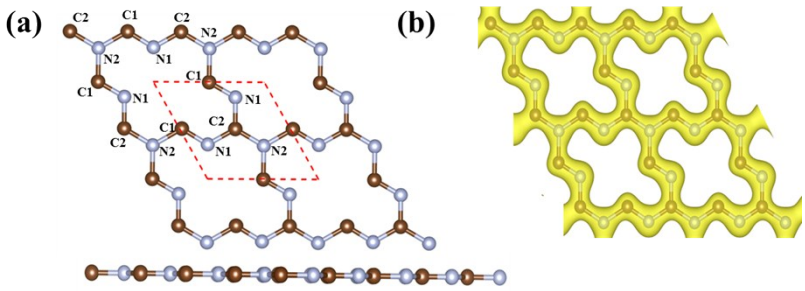

Figure S1: (a) Optimized structure of gt-C_3N_3 (top and side views) and (b) charge density of gt-C_3N_3 (Isosurface value is 0.18 e.Å^{-3}).

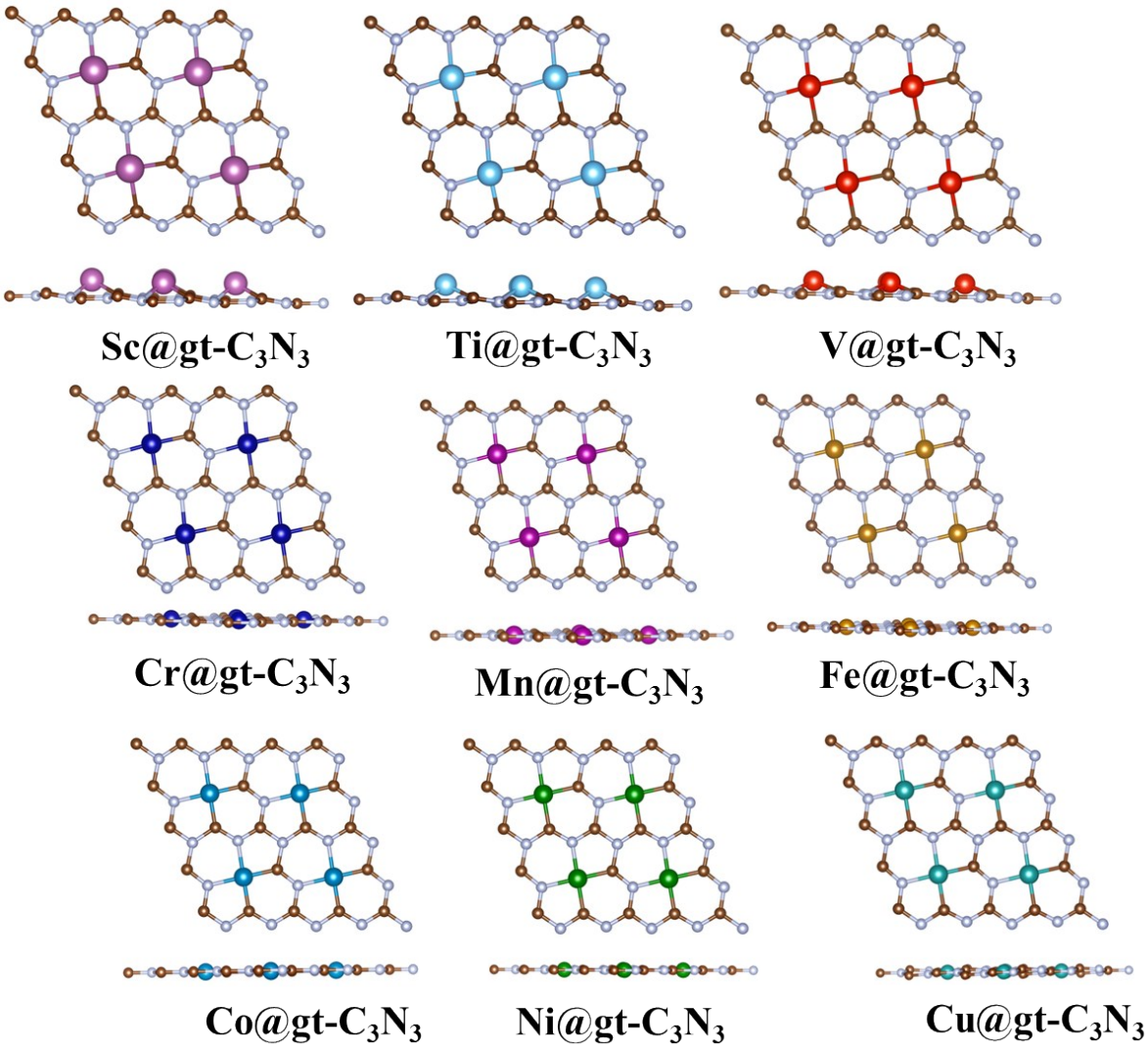

Figure S2: Optimized structures (top and side views) of TM@gt-C_3N_3 (TM = Sc to Cu) structures.

Table S1: Bond lengths and net effective charges calculated from Bader Charge analysis of gt-C_3N_3 and TM@gt-C_3N_3 (See Figure 1 in the manuscript for atom numbering)

Compound	Bond length (Å)		Net Effective Charge		
			C	N	TM
gt-C_3N_3		C2-N1 = 1.33 C2-N2 = 1.39 C1-N1 = 1.27 C1-N2 = 1.41	C1= +0.98 C2= +1.57	N1=-1.26 N2=-1.01	
Sc@gt-C_3N_3	Sc-N= 2.12 Sc-C= 2.15	C2-N2 = 1.44 C2-N1 = 1.35 C1-N1 = 1.36 C1-N2 = 1.43	C1= +0.55 C2 = +1.36	N1= -1.31 N2= -1.12	Sc = +1.44
Ti@gt-C_3N_3	Ti-N= 2.05 Ti-C= 2.06	C2-N2 = 1.42 C2-N1 = 1.35 C1-N1 = 1.36 C1-N2 = 1.41	C1= +0.48 C2 = +1.39	N1= -1.30 N2= -1.11	Ti = +1.33
V@gt-C_3N_3	V-N= 2.01 V-C= 1.99	C2-N2 = 1.43 C2-N1 = 1.35 C1-N1 = 1.36 C1-N2 = 1.42	C1= +0.53 C2 = +1.39	N1= -1.29 N2= -1.11	V = +1.24
Cr@gt-C_3N_3	Cr-N= 1.97 Cr-C= 1.94	C2-N2 = 1.44 C2-N1 = 1.35 C1-N1 = 1.34 C1-N2 = 1.42	C1= +0.06 C2 = +1.97	N1= -1.32 N2= -1.07	Cr = +1.62
Mn@gt-C_3N_3	Mn-N= 1.94 Mn-C= 1.90	C2-N2 = 1.43 C2-N1 = 1.36 C1-N1 = 1.35 C1-N2 = 1.42	C1= +0.06 C2= +1.99	N1= -1.32 N2= -1.15	Mn =+1.68
Fe@gt-C_3N_3	Fe-N= 1.92 Fe-C= 1.84	C2-N2 = 1.41 C2-N1 = 1.36 C1-N1 = 1.36 C1-N2 = 1.42	C1= +0.07 C2= +2.00	N1= -1.27 N2= -1.17	Fe = +1.57
Co@gt-C_3N_3	Co-N= 1.90 Co-C= 1.79	C2-N2 = 1.39 C2-N1 = 1.35 C1-N1 = 1.35 C1-N2 = 1.42	C1= +0.72 C2= +1.50	N1= -1.23 N2= -1.19	Co = +0.66
Ni@gt-C_3N_3	Ni-N= 1.89 Ni-C= 1.83	C2-N2 = 1.39 C2-N1 = 1.35 C1-N1 = 1.34 C1-N2 = 1.40	C1= +0.79 C2= +1.51	N1= -1.25 N2= -1.21	Ni = +0.62
Cu@gt-C_3N_3	Cr-N= 1.93 Cr-C= 1.89	C2-N2 = 1.41 C2-N1 = 1.35	C1= +0.78 C2= +1.46	N1= -1.27 N2= -1.20	Cu= +0.72

C1-N1 = 1.33 C1-N2 = 1.40

Text S1. Formation Energy (E_f), Binding Energy (E_B) and Cohesive Energy (E_{coh}) Calculations:

The N-vacancy formation energy is calculated for g-C_3N_3 system with the help of the following equation.

$$E_{N\text{-}vacancy} = [E_{gt\text{-}C3N4} - (E_{gt\text{-}C3N3} + \mu_N)] \quad (1)$$

Here, $E_{TM@g\text{-}C3N4}$ is the total energy of TM@gt-C_3N_4, $E_{g\text{-}C3N3}$ is the total energy of gt-C_3N_3 sheet, and μ_N represents the chemical potential of nitrogen (N). μ_N is calculated from the total energy of an isolated N_2 molecule.

The formation energy (E_f) is calculated for each TM embedding in the pore of gt-C_3N_3 (Figure 1) using the following equation:

$$E_f = [E_{TM@g\text{-}C3N3} - (E_{gt\text{-}C3N3} + \mu_{TM})] \quad (2)$$

where $E_{TM@g\text{-}C3N3}$ is the total energy of TM@gt-C_3N_3, $E_{g\text{-}C3N3}$ is the total energy of gt-C_3N_3 sheet, and μ_{TM} represents the chemical potential of TM in their respective bulk structure. The chemical potentials of Cr (μ_{Cr}), Mn (μ_{Mn}), and Fe (μ_{Fe}) are calculated from their most stable crystals such as Cr in bcc,[1] Mn in cubic,[2] and Fe in bcc,[3] respectively.

We have also calculated the binding energy (E_B) of TM in the pore of g-C_3N_3 using the following equation:

$$E_B = E_{gt\text{-}C3N3+TM} - (E_{gt\text{-}C3N3} + E_{TM}) \quad (3)$$

where, E_{TM} represents the total energy of the isolated atom.

The cohesive energy of a solid is the energy required to dissociate the solid into their isolated atomic species. It is calculated by using the following equation:

$$E_{coh} = E_{Solid} - \sum_A E_A^{isolated} \quad (4)$$

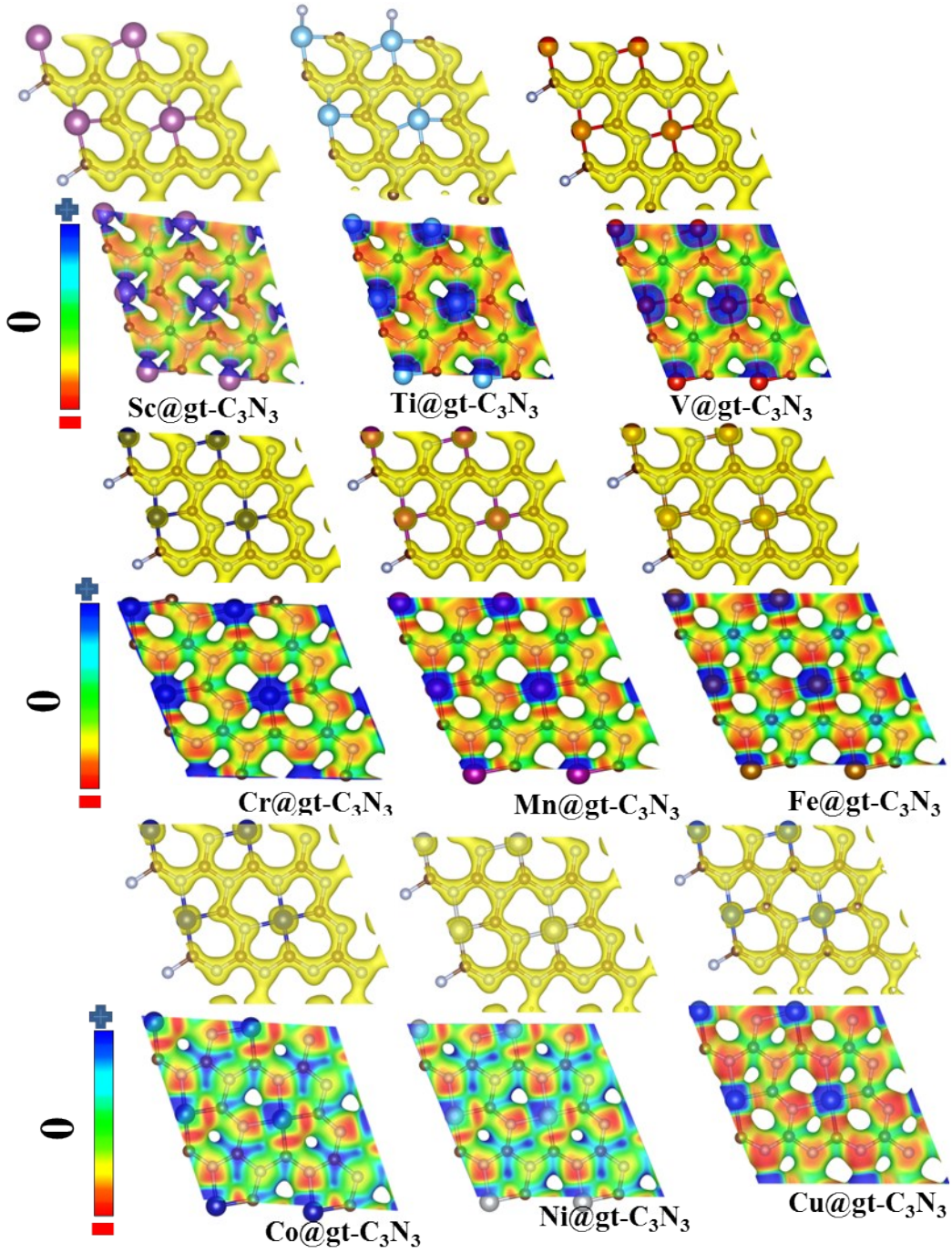

Figure S3: Total electron density (Isosurface value: 0.18 e.Å^{-3}) and electrostatic potentials (ESP) plots (Isosurface value: 0.03 e.Å^{-3}) of TM@gt-C_3N_3 (Sc to Cu). The blue and red colours denote less and more electron dense area in the electrostatic potential surface.

Table S2: Binding energy (E_B/TM), formation energy (E_F), cohesive energy of TM bulk (E_{Coh}/atom) and phonon frequency of TM@gt-C_3N_3 systems. (TM = Sc to Cu)

Systems (TM@gt-C_3N_3)	E_B /TM (eV)	E_F (eV)	E_{Coh} (eV)	Imaginary Frequency (*i*)	
				THz	cm^{-1}
Sc	-3.81	3.22	-4.11	1.61	53.76
Ti	-3.72	4.08	-5.02	1.73	57.80
V	-5.95	2.60	-5.56	0.79	26.31
Cr	-9.50	-1.81	-4.27	0.005	0.16
Mn	-8.26	-1.32	-3.12	0.012	0.42
Fe	-8.10	-1.17	-4.46	0.013	0.45
Co	-6.81	0.94	-4.62	1.36	45.45
Ni	-5.22	1.07	-4.67	0.96	32.07
Cu	-3.73	1.04	-3.75	0.50	16.69

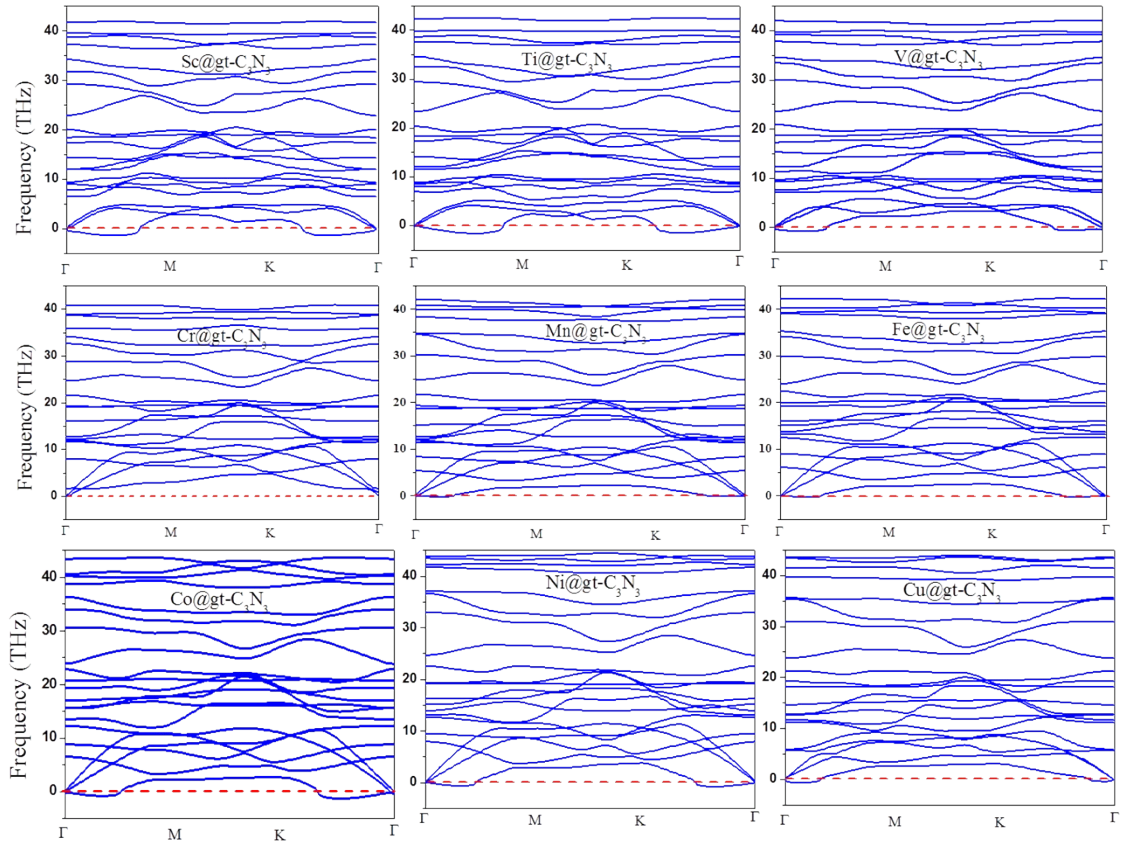

Figure S4: Phonon band structures of TM@gt-C_3N_3 (TM = Sc to Cu)

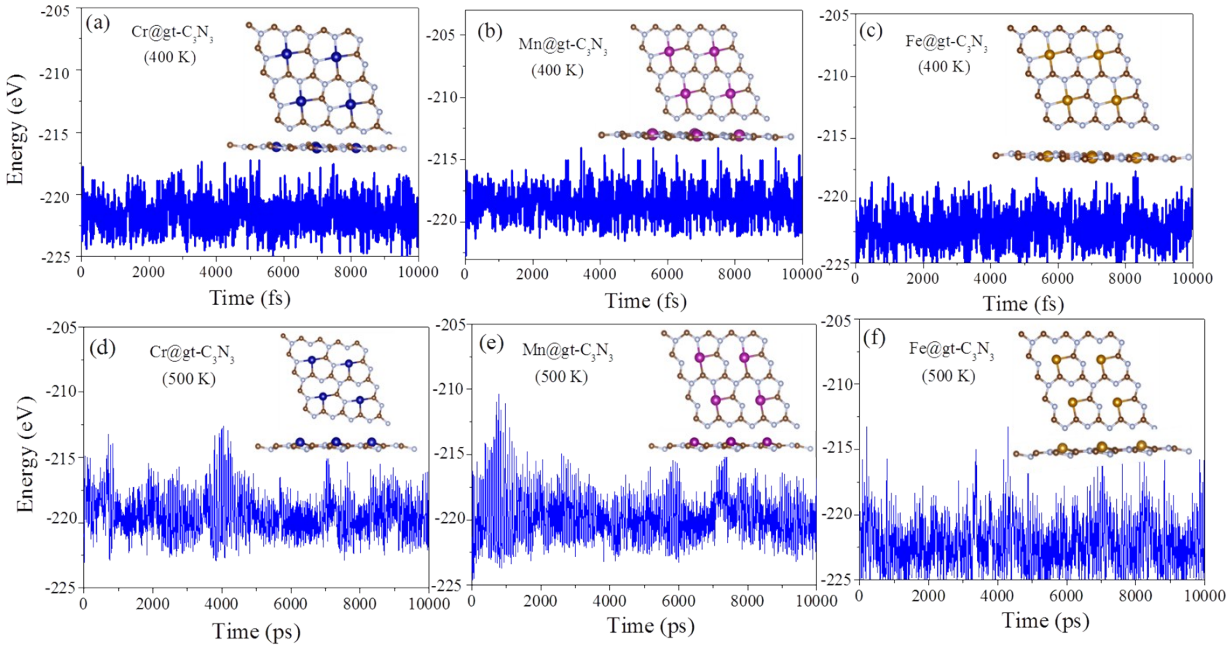

Figure S5: Total energy fluctuation during AIMD simulations of Cr@gt-C_3N_3, Mn@gt-C_3N_3 and Fe@gt-C_3N_3 systems at 400 and 500 K. The structures represent the snapshot at 10 ps for each simulation.

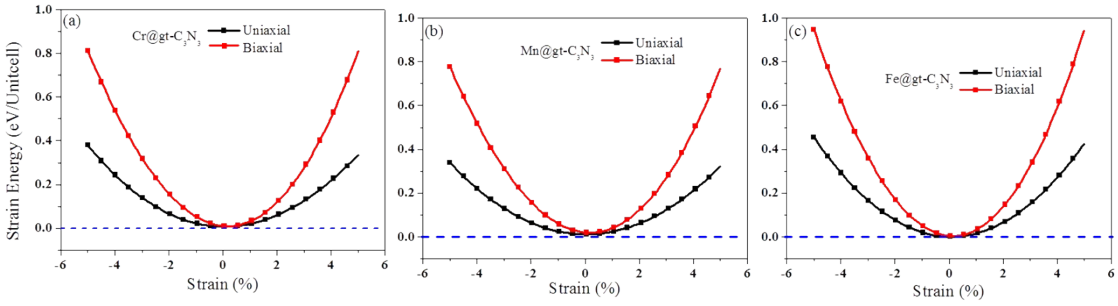

Figure S6: Strain energy of (a) Cr@gt-C_3N_3 (b) Mn@gt-C_3N_3 and (c) Fe@gt-C_3N_3 under in-plane uniaxial and equi-biaxial strains.

Table S3: Calculated Young's Modulus and Poisson's ratio of TM@gt-C_3N_3 by applying uniaxial and equi-biaxial strain.

Compound	Young's Modulus (GPa)	Poisson's Ratio	Elastic constants (GPa)
Cr@gt-C_3N_3	124.97	0.49	C_{11} =166.32 C_{12} = 82.92 C_{44} = 41.70
Mn@gt-C_3N_3	113.26	0.50	C_{11} =153.12 C_{12} = 78.12 C_{44} = 37.50
Fe@gt-C_3N_3	114.98	0.49	C_{11} =153.01 C_{12} = 76.28 C_{44} = 38.20

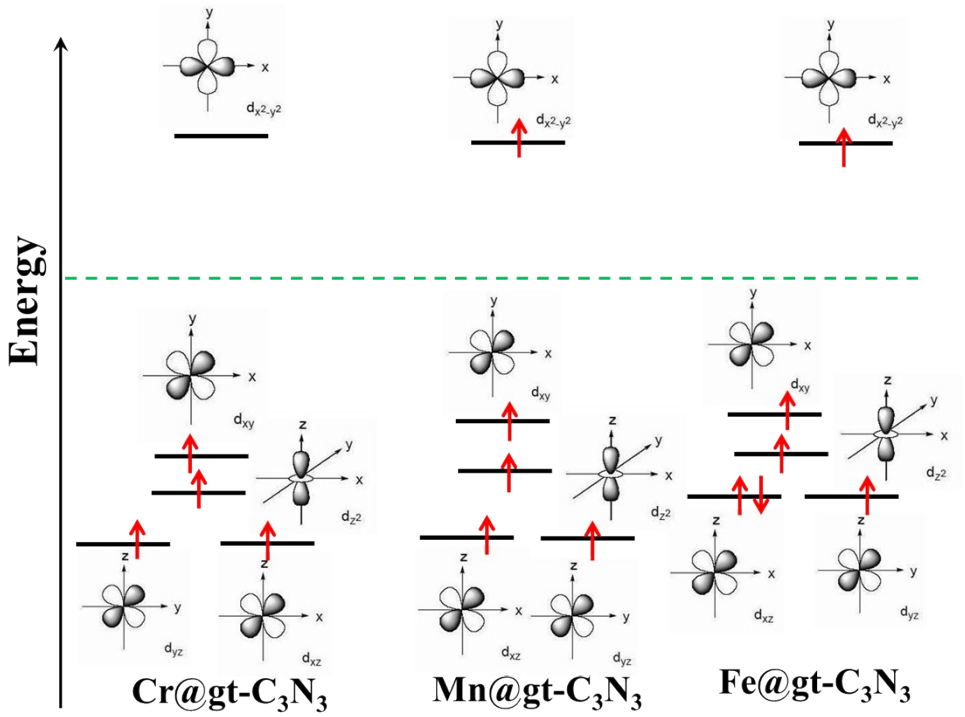

Figure S7. d-orbital splitting energy diagram for Cr, Mn and Fe@gt-C_3N_3 systems.

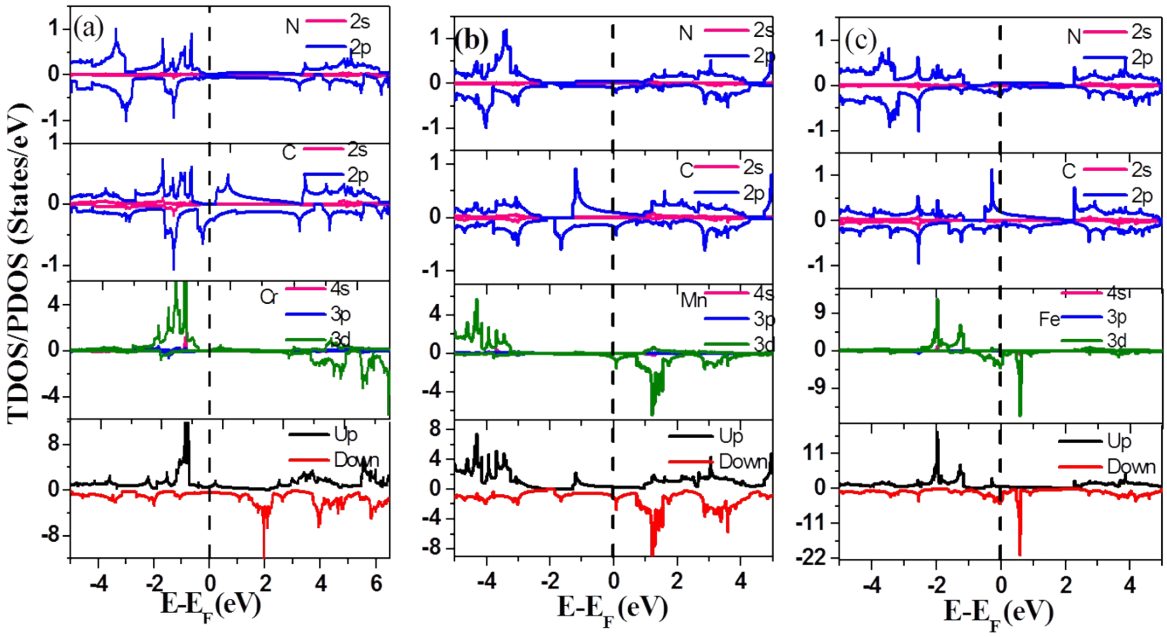

Figure S8: (a) TDOS and pDOS plot of (a) Cr@gt-C_3N_3, (b) Mn@gt-C_3N_3 and (c) Fe@gt-C_3N_3 (Fermi level is shifted to zero and indicated by a black dashed line).

Table S4: Exchange energy (E_{ex}) and Curie temperature value of TM@gt-C_3N_3 system.

Compound	Magnetic Moment/TM (μ_B)	Exchange energy (meV)/TM [$E_{ex} = E_{FM} - E_{AFM}$]	Energy Difference (meV)/TM ($E_{diff} = E_{FM} - E_{NSP}$)	Curie Temperature (T_C) in (K)	MAE in (meV)/TM (Magnetic Anisotropy Energy)
Cr@gt-C_3N_3	3.69	-312.99	-53.79	338* (205)[4](252)[5]	4.02[#] (2.40)[6](2.23)[7]
Mn@gt-C_3N_3	4.75	-307.74	-46.13	328	2.44
Fe@gt-C_3N_3	3.85	-303.55	-75.21	326	1.19

*Cr@gt-C_3N_3 shows higher Curie tempareture compare to first row transition metal incorporated carbon nitride systems such as V-g-C_3N_4 [4] and Cu-gt-C_3N_4.[5] In fact, Cr@gt-C_3N_3 has higher MAE compared to the previously reported Fe embedded graphyne[6] and Co nanowaires systems.[7] The previous studies on carbon nitride based systems did not report MAE and thus we could not comapare with carbon nitride based systems.

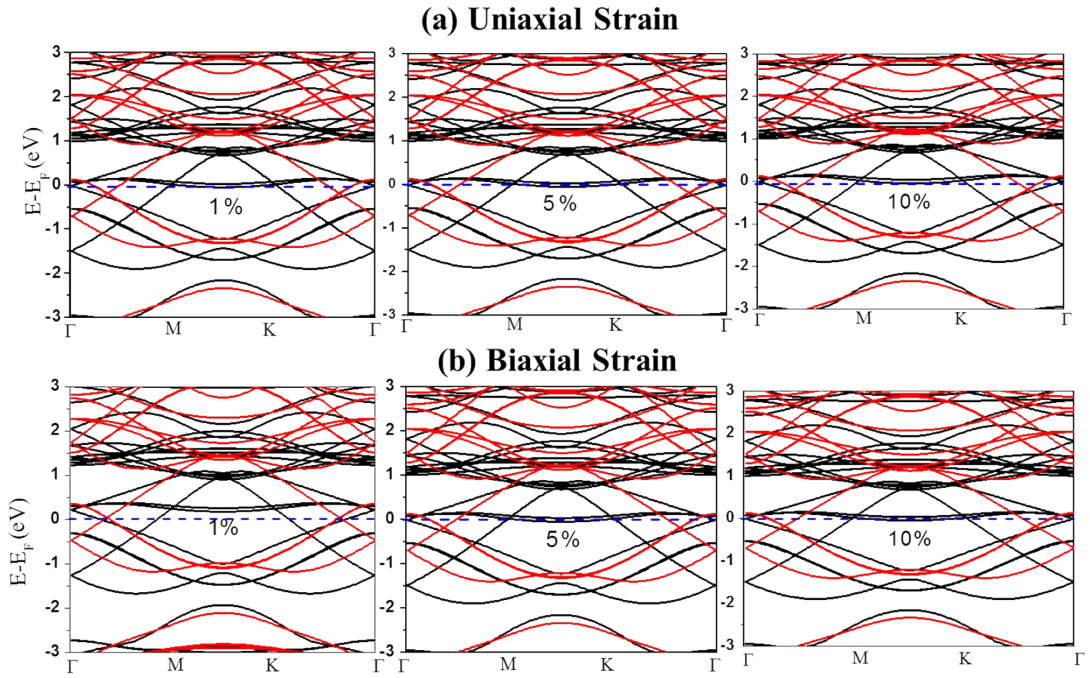

Figure S9. Band structures of Mn@gt-C_3N_3 by applying 1%, 5% and 10% (a) uniaxial and (b) biaxial tensile strain. The Fermi level is set to zero and indicated by a blue dashed line.

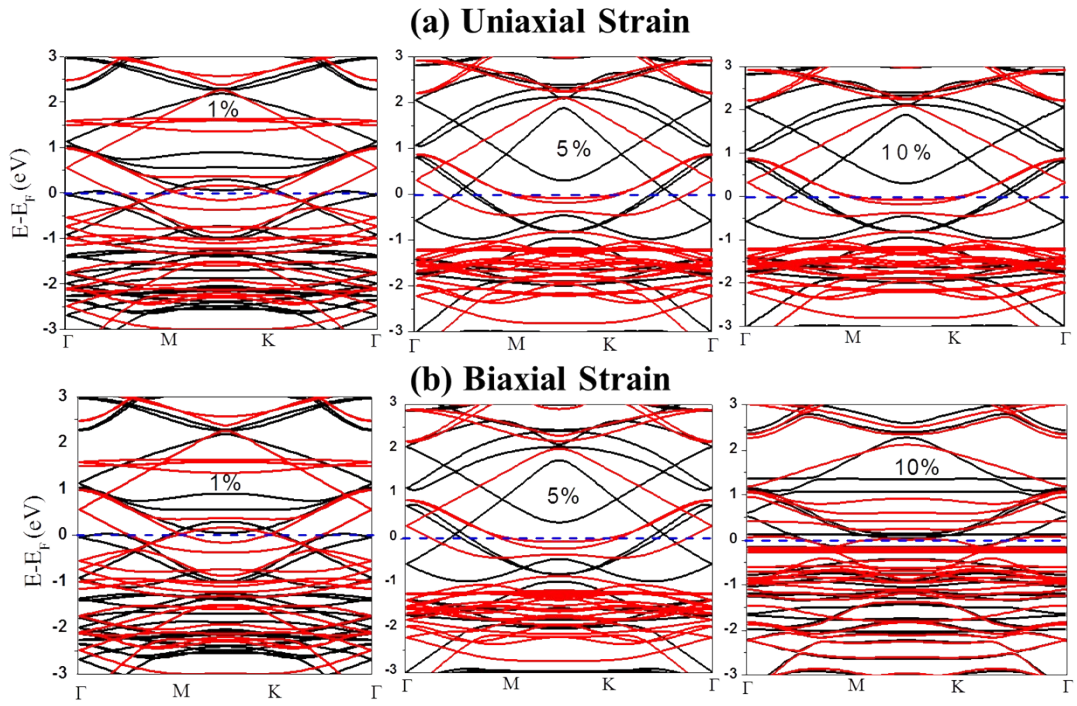

Figure S10. Band structures of Fe@gt-C_3N_3 by applying 1%, 5% and 10% (a) uniaxial and (b) biaxial tensile strain. The Fermi level is set to zero and indicated by blue dashed line

Text S2. Calculation of Magnetic Anisotropy Energy (MAE)

The magnetic anisotropy energy (MAE) is calculated by applying the torque approach.[8-9] Non-collinear self-consistent calculations (including spin orbit coupling) are performed in the z, y and x axis magnetization directions, respectively. MAE originates from the perpendicular and in plane contribution of spin orbit coupling (SOC), which can be expressed in terms of angular momentum operators L_x, L_y or L_z. So the contribution of different spins (up '↑↑' and down '↓↓') can be expressed by the second order perturbation equation.[10]

$$MAE = \xi^2 \sum_{o,u} \frac{|<o|L_Z|u>|^2 - |<o|L_X|u>|^2}{E_u - E_o}$$

Here, o and u represent the occupied and unoccupied electronic states, respectively. The E_o and E_u in the denominator are their respective band energies. L_Z and L_X are the angular momentum operators along Z and X axis, and ξ denotes the strength of the SOC. So, a

potential with good MAE for practical application should hold a high value of ξ. Then, the MAE is calculated using the following equation:

$$MAE = E_{S0} - E_{S1} \quad (5)$$

Where E_{S0} is the energy of the materials without employing any magnetic axis and E_{S1} is the energy in presence of an easy axis. Total energies are converged to a precision of 10^{-6} eV in MAE calculations.

Text S3.1 Mean Field Theory (MFT):

We have taken the MFT approach to calculate the Curie tempareture for the two dimentional TM@gt-C_3N_4 systems. This method has been previously used by Li et al.[11] for the Curie tempareture calculation for Mn-phthalocyanine (MnPc) system. The main idea behind MFT method is to replace all interactions to any one body with an average or effective interaction.[8] It reduces any multi-body problem into an effective one-body problem. The detailed partition function can be written as follows,

$$Z = \sum_{m = -M, -M+2, \ldots M-2, M} e^{\gamma J' m < M > / k_B T} \quad (6)$$

Here, 'J□' is the exchange parameter, 'γ' is the coordination number, 'm' is the ensemble-average magnetic moment, and 'M' is the calculated magnetic moment of TM.

Thus, the average spin of each magnet becomes,

$$<m> = \frac{1}{Z} \sum_{m = -M, -M+2, \ldots M-2, M} m \times e^{\gamma J' m < M > / k_B T} \quad (7)$$

Now, if we assume that, $P = \frac{\gamma J'}{k_B T}$, then the equation 5 becomes,

The above equation can be easily deducible when the parameter 'P' varies along with the static solution <m>. At the critical point,

$$P = P_c = \frac{\gamma J'}{k_B T_c} \qquad (8)$$

At this critical point, the phase transition of the system between ferromagnetic to paramagnetic occurs. This critical point is known as Curie temperature.

3.2 **Monte Carlo Simulations:**

Monte Carlo simulations involve generating a subset of configurations or samples, chosen using a random algorithm from a configuration space, according to a probability distribution or weight function. Observables are then computed as averages over the samples.[12]

One sample or configuration of the magnet is a particular assignment of spin values, say

$$s_1 = +1;\ s_2 = -1;\ s_3 = +1;\ \ldots\ldots\ldots\ldots\ldots;\ s_{Ns} = +1 \qquad (9)$$

in which each spin is set "up" or "down". According to statistical mechanics, the average value of an observable is got by weighting each configuration with the Boltzmann factor. For example, the average magnetization at some fixed temperature T is given by,

$$\langle M \rangle = \frac{\sum_{Config} M e^{-E/k_B T}}{\sum_{Config} e^{-E/k_B T}} \qquad (10)$$

At the Curie temperature (T_c) we expect a marked fluctuation in the magnetic moment (M).

Reference:

[1] R. G. Ross and W. Hume-Rothery, *J. Less-Common Metals*, 1963, **5**, 259.

[2] C. P. Gazzara, R. M. Middleton, R. J. Weiss, and E. O. Hall, *Acta Crystallogr*. 1967, **22**, 859.

[3] R. Kohlhaas, P. Donner, and N. Schmitz-Pranghe, Z. *Angew. Phys.,* **1967**, *23*, 245.

[4] Ghosh D.; Periyasamy G.; Pandeyc B.; Pati S. K. *J. Mater. Chem. C* **2014**, *2*, 7943–7951.

[5] Meng B.; Xiao W-z.; Wang L-l.; Yue, L.; Zhang S.; Zhang H-y.; *Phys. Chem. Chem. Phys.*, **2015**, *17*, 22136-22143.

[6] J. He, P. Zhou, N. Jiao, S. Y. Ma, K. W. Zhang, R. Z. Wang, and L. Z. Sun. *Sci. Rep* 2013, **4**, 04014.

[7] Hong J.; Wu R. Q.; *Phys. Rev. Lett*., 2006, **96**, 147201.

[8] Wang X.; Wu R.; Wang D. S.; Freeman A. J. *Phys. Rev. B: Condens. Matter Mater. Phys*., 1996, **54,** 61.

[9] Hu J.; Wu R. *Phys. Rev. Lett*., 2013, **110**, 097202.

[10] Wang D. S.; Wu R. Q.; Freeman A. J. *Phys. Rev. B: Condens. Matter Mater. Phys.,* 1993, **47**, 14932.

[11] X. Li, X. Wu, J. Yang. *J. Am. Chem. Soc*. 2014, **136**, 5664.

[12] D. P. Kroese, T. Brereton, T. Taimre, Z. I. Botev, *Comput. Stat.* 2014, **6**, 386.